https://doi.org/10.1016/j.mtener.2019.01.005

Inkjet Printed Pseudocapacitive Electrodes on Laser-Induced Graphene for Electrochemical Energy Storage

Guijun Li,[1] Zhengong Meng,[2] Jiasheng Qian,[1] Cheuk-Lam Ho,[2] Shu Ping Lau,[1] Wai-Yeung Wong,[2]* Feng Yan[1]*

1. Department of Applied Physics, Hong Kong Polytechnic University;
2. Department of Applied Biology and Chemical Technology, Hong Kong Polytechnic University

Abstract

Pseudocapacitance boosts the capacitance of supercapacitors by introducing additional redox sites with fast faradaic reactions. Although numerous reports have studied the application of battery-type materials for pseudocapacitive electrodes, how to control the faradaic redox to pseudocapacitive transition is still challenging. Here, we demonstrate the switching from battery-type to pseudocapacitance-type electrochemical energy storage by simply controlling the inkjet printing temperature. The pseudocapacitive electrodes printed above the boiling temperature of the solvent showed 75 times larger areal specific capacitance (1.2 mF/cm^2) than pristine graphene. The substrate temperature during inkjet printing can effectively tune the morphology of the pseudocapacitive additives by overcoming the influence of coffee ring effect. This work demonstrates a novel solution for tweaking the electrochemical behavior of supercapacitor electrode via modifying the evaporation condition of the solvent. This

approach can also be employed for the deposition of other functional materials via inkjet printing.

Introduction

With the development of emerging portable and wearable devices such as mobile phones, smart watches, wireless headphones, healthy monitoring devices and virtual reality sets, there are huge requirements for durable mobile powering sources for charging these devices.[1] Although microbatteries are dominating these markets, their poor charging speeds and limited lifetimes are dissatisfying.[2] The development of microsupercapacitors provide novel solutions for on-chip electronic devices with advanced features such as fast charging rates, long durability, and low costs. However, the native capacitance of supercapacitor based on electrical double layer capacitance (EDLC) was low due to their limited accessible surface areas.[3] In recent years, tremendous research efforts are focusing on the synthesis of novel supercapacitor electrode materials with pseudocapacitance, which can greatly increase the specific capacitance.[4-6] RuO_2 and MnO_2 nanoparticles have been widely studied for achieving high areal capacitance on microsupercapacitor devices.[7, 8] However, the methods for patterning such microsupercapacitors is costly, limiting their application for real production. For example, photolithography and post metal depositions have been used for fabricating on chip microsupercapacitor with areal capacitance up to 50 mF/cm^3.[9] However, both the lithography process and the use of noble metals as current collectors greatly increase the cost of the devices. Electrophoretic deposition has also been studied

for fabricating microsupercapacitors.[10] Nonetheless, these electrolyte-based processes generate additional wastes, and the long plating duration further increase the production time cost. Screen printing have also been applied for depositing the functional electrode materials onto current collectors; however, the unused inks within the undesired patterns also increase the overall cost.[11] Although these methods can be used to successfully fabricate supercapacitors with high performances, the involved costs greatly limit their actual application for mass production of practical microsupercapacitors.

At the same time, inkjet printing that delivers the drop-on-demand advantage can greatly save the cost for fabricating microsupercapacitor by depositing the functional materials only on the desired locations.[12, 13] Although the used materials might be expensive, the overall cost can be lowered because of the high efficient use of the materials compared with other methods.[14] Taking advantage of the computer aided design, the inkjet printing head can move along the desired path and deposit the electrode materials in both interdigital and in-plane configurations. High performance materials such as MnO_2 nanoparticles have been successfully inkjet-printed for microsupercapacitor devices, achieving areal density as high as 52.9 mF/cm^2.[15] RuO_2 have also been deposited onto gold current collectors via inkjet printing in the form of interdigitated configurations.[16] Unfortunately, the above inks are suspensions, rather than fully dissolved. The suspensions might be stable for short time storage; however, considering actual production processes of long durations, the inks would aggregate over time. The resulting precipitation of the inks would lead to either clogging of the

inkjet print heads, or the aggregation of the nanoparticles on the electrodes. Although frequent purging can technically avoid the clogging issue, the wasted inks during the purging process is in the contradiction to the concept of drop-on-demand.[17] In addition, the aggregated nanoparticle would form larger clusters than desired, making the electrolyte ions difficult to access, forming battery-type storage rather than pseudocapacitance.[18] These obstacles need to be fully considered for fabricating practical microsupercapacitor via inkjet printing. Although there are a range of materials with complete solubility in common organic solvents while keeping insolubility in aqueous solution, there is no report on taking advantages of these phenomenon for fabricating supercapacitors with these non-clogging inks.[19]

Graphene is an important electronic material with versatile applications.[20-24] Recently, low-cost laser induced graphene (LIG) has been developed for fabricating graphene-based microsupercapacitors.[25] These micro 3D structured electrodes provide both large surface areas as well as high electrical conductivity, offering novel solutions for in-plane supercapacitors. However, the native capacitance basing on the EDLC mechanism is low. Although electrical deposition of MnO_2 and FeOOH on these LIG can boost the capacitance, the electrodeposition sacrifices long process time and generate the waste pollutions.[26] Meanwhile, organic semiconductor materials are demonstrating growing functions in various electrochemical applications.[27-29] Transition metal coordinate complex with Co(II) and terpyridyl ligands are typical semiconductors for studying electrochemical mechanisms.[30] The Co(II) elements can be oxidized to Co(III) or reduced to CO(I) through redox reaction.[31] The terpyridyl

ligands on the Co(II) cores could enhance the electrochemical reaction in the hydrogen evaluation reaction.[32] Herein, we report the fabricating of nanostructured pseudocapacitive electrode on LIG current collector via one-step inkjet printing. An organic semiconductor bis-terpyridyl based molecular cobalt complexes (TPy-Co) was synthesized and dissolved in DMF as an ink. TPy-Co is a suitable material for electrode modification because it is highly soluble in some organic solvents (such as DMF, methanol, etc) and non-soluble in aqueous electrolytes. The non-clogging TPy-Co solution is inkjet-printed on the LIG current collectors at different temperatures. When the temperature is above the boiling point of DMF, stable pseudocapacitive electrodes in aqueous and gel-type electrolytes are obtained, leading to 75 times higher capacitance over the pristine LIG.

Results and Discussion

Inkjet-printed solutes might form distinct distributions on the LIG substrate with altered depositing conditions. The behaviors of electrolytic ions on LIG with different morphologies of additives are illustrated in Scheme 1, with their corresponding cyclic voltammetry (CV) shapes. For pristine porous graphene without any additives, ions from the electrolytes would settle along their edges as Electrical Double Layer Capacitance (EDLC), forming typical square shape CV slopes shown in Schema 1a. When additives at large sizes are added on to the graphene, many surface areas of the pristine graphene are wrapped as illustrated in Scheme 1b, isolating the accesses of the electrolyte ions. Although the additives can increase the total capacitance due to the

redox peaks, the inclusive CV behavior is still battery type, rather than pseudocapacitance.[33] If the additives are sufficiently small compared to the LIG structures, the electrolyte ions can still possess appropriate contacts with pristine graphene and the additives surfaces. A pseudocapacitance behavior, including a quasi-square shape representing the EDLC and slight redox peaks representing the faradaic reactions, is illustrated in Scheme 1c. With different morphologies of additives, the CV shapes of graphene-based supercapacitor would diverge significantly.

The overall process for fabricating the pseudocapacitive microsupercapacitor with laser scribing of polyimide and inkjet printing of TPy-Co was schematically illustrated in Figure 1. First, a polyimide film is placed on to the working area of a CO_2 laser machine, as illustrated in Figure 1a. Secondly, the CO_2 laser beam is scanned across the polyimide film in the path as computer aided designs, and the color of the treated areas will turn to black graphene as shown in Figure 1b. Thirdly, the laser scribed graphene film was placed onto a heated substrate up to 188^{o}C before the TPy-Co ink was inkjet-printed onto the graphene, along the same computer designed path as shown in Figure 1c. Finally, two such processed electrodes and the gel electrolyte was assembled in the sandwiched type as a supercapacitive device as Figure 1d.

Among the above steps, the inkjet printing process will predominantly influence the overall quality of pseudocapacitive performance. Coffee ring effects are the foremost obstacles determining the distributions of the solute within a single droplet.[34, 35] For a normal coffee-ring condition, the temperature of the substrates is significantly lower than the boiling point of the solvent. The droplet would evaporate slowly,

allowing the solute to assemble along the contour near the evaporation lines, as illustrated in Figure 2a. After the solvent is completely dried, the solute will distribute along the outer rings of the as-coated droplet, as the coffee ring shape. However, these coffee-ring distributions can be broken when the substrate temperature is significantly high. After the droplet arrives the hot substrate, the solvent will start to evaporate severely. The fast evaporation process would break the equilibrium of the surface tension at the contour.[36] As a result, the solutes tend to distribute randomly due to the thermal turbulence, as illustrated in Figure 2b, without the influence of surface tension. To verify this hypothesis, the morphologies of the dried solute at different temperatures were examined on flat surfaces (glass slides and silicon wafer) and porous LIG (actual electrodes), respectively. For the samples printed at room temperatures, the solute would form typical coffee rings patterns (Figure S1). Most solute formed on the edges of the droplet while almost no solute was observed at the center areas. A typical morphology of the dried solutes on the edge parts was shown in Figure 2c, indicating a highly aggregated state with solutes forming continuous blocks. These large blocks would contribute only to a battery-type faradaic effect rather than the pseudocapacitance. In contrary, the morphology of the solute printed at high temperature (Figure S2) show homogeneous distribution without aggregation, as shown in Figure 2d. As a typical supramolecular, the TPyCo possess the strong tendency to self-assembly under this drying condition.[37] These nano clusters smaller than 100 nm in diameter are within the proper size ranges for delivering pseudocapacitance.[38] The above distributions on glass substrates were also observed on printed LIG substrates

after inkjet printing in the same conditions. For room temperature printing, similar aggregated blocks were shown in Figure 1e. So, the coffee-ring effect induced gathering was preserved at the porous LIG, which was unfavorite for the pseudocapacitance. Meanwhile, isolated nano dots without aggregation were observed on LIG after printing at high temperature (measured to be 188^{o}C with IR detector) as shown in Figure 1f. The existence of the TPy-Co molecules on LIG were verified from the EDX and XPS characterization in the supplementary information. The above results indicate that the TPy-Co can form nanosized clusters on the LIG substrates, at optimized inkjet printing conditions. These tiny structures will facilitate the ions to enter for pseudocapacitive capacitance, rather than battery-type faradaic capacitance, as verified in the following electrochemical studies.

The electrochemical characterizations of the pristine LIG, and with TPy-Co additive printed at different temperatures are shown in Figure 3. The cyclic voltammetry (C-V) profiles of samples with different inkjet printing conditions are shown in Figure 3a, at scanning rates of 100 mV. The pristine LIG in neutral 5M LiCl aqueous electrolyte shows a typical EDLC rectangular shape. After the TPy-Co ink was inkjet-printed at room temperature, the CV showed significant redox peak from 0.6V to 0.9 V, indicating the battery-type storage.[39] Meanwhile, the CV profile of the TPy-Co inkjet-printed at high temperature behaves a typical pseudocapacitive curve: a quasi-square curve with redox peaks near 0 V and 0.9 V. The peak intensity at 0 V is slightly larger than the other redox peaks, which is due to the stronger self-exchange for the Co(II/I) reaction.[30] In addition, the effective area of TPy-Co printed at high temperature

is significantly larger than those of the pristine LIG and TPy-Co printed at room temperature, indicating drastically larger capacitance for the TPy-Co electrodes printed at high temperature. Thus, the optimized inkjet printing can indeed increase the capacitance by introducing pseudocapacitive additives. Besides enhanced capacitance, the TPy-Co additives can also optimize the supercapacitor performance by increasing the electrical conductivity. As illustrated in Figure 3b, the effective series resistance (ESR) of the pristine LIG is around 48 Ω. However, with the additives of TPy-Co, the ESR can be significantly lowered to 7 Ω and 11 Ω for the inkjet-printed samples at high and room temperatures, respectively. So, the supercapacitor performances were further optimized by the nanosized TPy-Co additives with reduced ESR. The reduced ESR also presented a smaller IR drop (12 mV) in the galvanostatic charge/discharge(GCD) curves at 0.1 $mA \bullet cm^{-2}$ in Figure 3c. In addition, the advantage of introducing pseudocapacitance was also demonstrated, with longer discharging time at same scanning rates. The pristine graphene took only 0.5 second for the full charge and discharge cycle. While the LIG sample after inkjet-printed at room temperatures took 1 second for the same duty, indicating higher capacity with the same areal. And the LIG sample with high inkjet printing temperature possess even longer charge and discharging duration over 19 seconds. The specific areal capacitances with these samples were plotted in Figure 3d, indicating the optimized inkjet printing temperature can boost the corresponding capacitance by 75 times compared to pristine LIG and 15 times compared to TPy-Co printed at room temperature. The optimized supercapacitor can also power up a LED with in-series configuration, as shown in Figure 3e.

Pseudocapacitive additives are crucial for supercapacitor devices, which can increase specific capacitance, without sacrificing the fast charging/discharging performance.[40] Although the EDLC is the ideal case for supercapacitor energy storage, energy can only be stored at the surface of the electrodes. Even with the highest surface area accessible, the maximum specific capacitance can't exceed 400 F/g.[41] With pseudocapacitive additives, however, the overall specific capacitance can easily reach a few thousand farads per gram.[42] Meanwhile, the identification of the pseudocapacitance from the battery-type faradaic redox is challenging. With a single synthesis or deposit method, usually one type of storage can be achieved, being either pseudocapacitive or faradaic redox. Using distinctive synthesis methods, however, the resulted products can be quite different in the crystalline structures, chemical compositions, and microporous architectures, etc.[43] Thus, the current study of pseudocapacitive, with transition from electrical double layer supercapacitance to redox, will benefit the understanding of such storage mechanisms.[44]

By tuning the deposition parameters, this work demonstrates the transition among three different storage mechanisms: EDLC, pseudocapacitive, and faradaic redox. By increasing the inkjet printing temperatures, the morphologies of the additives were considerably modified, from aggregated blocks to nanosized isolated distributions. The resulting inkjet-printed aggregations and nano-spheres showed battery-type redox and pseudocapacitive performances, respectively. The pseudocapacitance not only maintain the fast charging/discharging features, but also boost the overall specific areal capacitance by providing more accessible surfaces areas compared to the ELDC and

redox types.

This inkjet printing of fully-dissolved pseudocapacitive additives for fabricating microsupercapacitors also have advantages over existing methods. Electroplating of MnO_2 on laser induced graphene has boosted the capacitance of interdigitate microsupercapacitor for hundreds of times.[45] However, the duration for such plating takes hours to finish one sample, which would significantly increase the overall processing time. In addition, electroplating also generates additional wastes, which is not environmental friendly. Meanwhile, the inkjet printing process is a fast and drop-on-demand method, which can effectively tackle the long processing durations and waste issues. The current full-dissolved TPyCo inks also demonstrate advantages over existing dispersed inks due to their high solubility. [46]

Although micro-supercapacitors with enhanced specific capacity were demonstrated using the inkjet printing of the TPy-Co ink at high temperatures, there are still some limitations of the current study. Compared to other pseudocapacitive materials, the specific capacitances of TPy-Co additives are relatively low. Future works can be performed with other metal complex materials of higher specific capacitance.[47] The influence of the cobalt valance states on the supercapacitor performance is not fully understood yet. A more fundamental study with a Co(III) state inks can be compared according to the current Co(II) inks.[48] For inkjet printing of other materials, the morphology of the dried inks should also be explored to demonstrate the versatility of this method for controlling the morphology for inkjet printing at various temperatures. The laser scribing and inkjet printing can be designed with arbitrary

patterns, which can be easily manufactured into any shapes required for the internet of things (IoT).[49]

Conclusion

A novel strategy combining laser induced graphene and inkjet printing of dissolved inks for fabricating high-performance supercapacitor was developed. Arbitrary shapes of the electrodes can be made with computer aided designs. The inkjet printing of the pseudocapacitive materials can boost the specific capacitance by 75 times without sacrificing the charging and discharging rates. This method opens the window of controlling the microstructure of inkjet-printed pseudocapacitive electrodes by changing deposition temperature. The TPy-Co inks demonstrate a novel family of organic semiconductor materials, with transition metal cores and organic ligands, can work as pseudocapacitive electrodes for supercapacitor applications.

Experimental

Ink synthesis: The bis-substituted cobalt(II) complex of TPy-Co was synthesized according to the previous literature.[50] The tridentate ligand terpyridine and cobalt dichloride with accurate stoichiometric ratios were stirred vigorously in methanol at room temperature for 2 h, and then excess ammonium hexafluorophosphate (NH_4PF_6) aqueous solution was added to exchange the anion. The precipitate was filtered and washed by water, cold methanol, and then purified by crystallization by slow evaporation of diethyl ether into acetonitrile solution. The complex is paramagnetic, the peaks in 1H NMR spectrum were existed at up to ca. 120 ppm. The TPy-Co was dissolved in DMF with concentration at 3 mg/mL.

Inkjet printing: The inkjet printing of the TPy-Co ink was performed using a Microdrop MD-K-130 with a custom-made X-Y moving stage. The substrate is heated up with a hotplate, and the actual temperature during printing was measured to be 188 ^{o}C.

Characterization: The microstructures of the samples were characterized using a Tescan MAIA3 Field Emission Scanning Electron Microscope (FESEM). X-ray Photoemission Spectrometry (XPS) with SKL-12 spectrometer and an Mg Ka X-ray source was used for the chemical information characterization. The Raman spectra was characterized with a LabRAM HR 800 Raman Spectrometer using a 488 nm laser source. The electrochemical measured was performed using a Princeton VersaSTAT III electrochemical station.

Acknowledgement

G. Li and Z. Meng contributed equally to this work.

Reference

1. A. M. Zamarayeva, A. E. Ostfeld, M. Wang, J. K. Duey, I. Deckman, B. P. Lechene, G. Davies, D. A. Steingart and A. C. Arias, *Sci. Adv.*, 2017, **3**, e1602051.
2. W. Wang, M. Tian, A. Abdulagatov, S. M. George, Y. C. Lee and R. G. Yang, *Nano Lett.*, 2012, **12**, 655-660.
3. D. S. Yu, K. Goh, H. Wang, L. Wei, W. C. Jiang, Q. Zhang, L. M. Dai and Y. Chen, *Nat. Nanotechnol.*, 2014, **9**, 555-562.
4. J. T. Mefford, W. G. Hardin, S. Dai, K. P. Johnston and K. J. Stevenson, *Nat. Mater.*, 2014, **13**, 726-732.
5. V. Augustyn, J. Come, M. A. Lowe, J. W. Kim, P. L. Taberna, S. H. Tolbert, H. D. Abruna, P. Simon and B. Dunn, *Nat. Mater.*, 2013, **12**, 518-522.
6. T. Brezesinski, J. Wang, S. H. Tolbert and B. Dunn, *Nat. Mater.*, 2010, **9**, 146-151.
7. Z. Wen, M. H. Yeh, H. Y. Guo, J. Wang, Y. L. Zi, W. D. Xu, J. N. Deng, L. Zhu,

X. Wang, C. G. Hu, L. P. Zhu, X. H. Sun and Z. L. Wang, *Sci. Adv.*, 2016, **2**, e1600097.
8. X. Y. Lang, A. Hirata, T. Fujita and M. W. Chen, *Nat. Nanotechnol.*, 2011, **6**, 232-236.
9. J. Chmiola, C. Largeot, P. L. Taberna, P. Simon and Y. Gogotsi, *Science*, 2010, **328**, 480-483.
10. D. Pech, M. Brunet, H. Durou, P. H. Huang, V. Mochalin, Y. Gogotsi, P. L. Taberna and P. Simon, *Nat. Nanotechnol.*, 2010, **5**, 651-654.
11. Y. F. Xu, M. G. Schwab, A. J. Strudwick, I. Hennig, X. L. Feng, Z. S. Wu and K. Mullen, *Adv. Energy Mater.*, 2013, **3**, 1035-1040.
12. D. McManus, S. Vranic, F. Withers, V. Sanchez-Romaguera, M. Macucci, H. F. Yang, R. Sorrentino, K. Parvez, S. K. Son, G. Iannaccone, K. Kostarelos, G. Fiori and C. Casiraghi, *Nat. Nanotechnol.*, 2017, **12**, 343-350.
13. H. Sirringhaus, T. Kawase, R. H. Friend, T. Shimoda, M. Inbasekaran, W. Wu and E. P. Woo, *Science*, 2000, **290**, 2123-2126.
14. H. Yan, Z. H. Chen, Y. Zheng, C. Newman, J. R. Quinn, F. Dotz, M. Kastler and A. Facchetti, *Nature*, 2009, **457**, 679-U671.
15. Y. J. Lin, Y. Gao and Z. Y. Fan, *Adv. Mater.*, 2017, **29**, 1701736.
16. P. C. Chen, H. T. Chen, J. Qiu and C. W. Zhou, *Nano Research*, 2010, **3**, 594-603.
17. S. Fathi, P. Dickens, K. Khodabakhshi and M. Gilbert, *Journal of Manufacturing Science and Engineering-Transactions of the Asme*, 2013, **135**, 011009.
18. L. Johnson, C. M. Li, Z. Liu, Y. H. Chen, S. A. Freunberger, P. C. Ashok, B. B. Praveen, K. Dholakia, J. M. Tarascon and P. G. Bruce, *Nature Chem.*, 2014, **6**, 1091-1099.
19. J. Huang, K. C. Yung, Z. Meng, D. T. C. Ang and G. Li, *IEEE Magnetics Letters*, 2017, **8**, 2104405.
20. C. Xie, C. Mak, X. M. Tao and F. Yan, *Adv. Funct. Mater.*, 2017, **27**.
21. Z. K. Liu, P. You, C. Xie, G. Q. Tang and F. Yan, *Nano Energy*, 2016, **28**, 151-157.
22. P. You, Z. K. Liu, Q. D. Tai, S. H. Liu and F. Yan, *Adv. Mater.*, 2015, **27**, 3632-3638.
23. Z. K. Liu, S. P. Lau and F. Yan, *Chem. Soc. Rev.*, 2015, **44**, 5638-5679.
24. J. H. Li, L. Y. Niu, Z. J. Zheng and F. Yan, *Adv. Mater.*, 2014, **26**, 5239-5273.
25. J. Lin, Z. W. Peng, Y. Y. Liu, F. Ruiz-Zepeda, R. Q. Ye, E. L. G. Samuel, M. J. Yacaman, B. I. Yakobson and J. M. Tour, *Nat. Commun.*, 2014, **5**, 5714.
26. L. Li, J. B. Zhang, Z. W. Peng, Y. L. Li, C. T. Gao, Y. S. Ji, R. Q. Ye, N. D. Kim, Q. F. Zhong, Y. Yang, H. L. Fei, G. D. Ruan and J. M. Tour, *Adv. Mater.*, 2016, **28**, 838-845.
27. S. H. Liu, Y. Fu, G. J. Li, L. Li, H. K. W. Law, X. F. Chen and F. Yan, *Adv. Mater.*, 2017, **29**.
28. Y. Fu, N. X. Wang, A. N. Yang, H. K. W. Law, L. Li and F. Yan, *Adv. Mater.*, 2017, **29**.

29. J. H. Li, D. Q. Liu, Q. Miao and F. Yan, *J. Mater. Chem.*, 2012, **22**, 15998-16004.
30. D. A. Buttry and F. C. Anson, *J. Am. Chem. Soc.*, 1983, **105**, 685-689.
31. P. W. Du, K. Knowles and R. Eisenberg, *J. Am. Chem. Soc.*, 2008, **130**, 12576-+.
32. S. Aroua, T. K. Todorova, V. Mougel, P. Hommes, H. U. Reissig and M. Fontecave, *Chemcatchem*, 2017, **9**, 2099-2105.
33. X. L. Dong, L. Chen, J. Y. Liu, S. Haller, Y. G. Wang and Y. Y. Xia, *Sci. Adv.*, 2016, **2**.
34. P. J. Yunker, T. Still, M. A. Lohr and A. G. Yodh, *Nature*, 2011, **476**, 308-311.
35. R. D. Deegan, O. Bakajin, T. F. Dupont, G. Huber, S. R. Nagel and T. A. Witten, *Nature*, 1997, **389**, 827-829.
36. T. P. Bigioni, X. M. Lin, T. T. Nguyen, E. I. Corwin, T. A. Witten and H. M. Jaeger, *Nat. Mater.*, 2006, **5**, 265-270.
37. D. R. Blasini, S. Flores-Torres, D. M. Smilgies and H. D. Abruna, *Langmuir*, 2006, **22**, 2082-2089.
38. M. Toupin, T. Brousse and D. Belanger, *Chem. Mater.*, 2004, **16**, 3184-3190.
39. K. Takada, G. D. Storrier, J. I. Goldsmith and H. D. Abruna, *J. Phys. Chem. B*, 2001, **105**, 2404-2411.
40. E. Mourad, L. Coustan, P. Lannelongue, D. Zigah, A. Mehdi, A. Vioux, S. A. Freunberger, F. Favier and O. Fontaine, *Nat. Mater.*, 2017, **16**, 446-454.
41. Y. W. Zhu, S. Murali, M. D. Stoller, K. J. Ganesh, W. W. Cai, P. J. Ferreira, A. Pirkle, R. M. Wallace, K. A. Cychosz, M. Thommes, D. Su, E. A. Stach and R. S. Ruoff, *Science*, 2011, **332**, 1537-1541.
42. C. Zhou, Y. W. Zhang, Y. Y. Li and J. P. Liu, *Nano Lett.*, 2013, **13**, 2078-2085.
43. J. W. Long, K. E. Swider, C. I. Merzbacher and D. R. Rolison, *Langmuir*, 2003, **19**, 2532-2532.
44. J. B. Mitchell, W. C. Lo, A. Genc, J. LeBeau and V. Augustyn, *Chem. Mater.*, 2017, **29**, 3928-3937.
45. C. L. Liu, D. Y. Gui and J. H. Liu, *Chem. Phys. Lett.*, 2014, **614**, 123-128.
46. J. S. Qian, H. Y. Jin, B. L. Chen, M. Lin, W. Lu, W. M. Tang, W. Xiong, L. W. H. Chan, S. P. Lau and J. K. Yuan, *Angewandte Chemie-International Edition*, 2015, **54**, 6800-6803.
47. X. Y. Chen, Y. Y. He, H. Song and Z. J. Zhang, *Carbon*, 2014, **72**, 410-420.
48. E. Fagadar-Cosma, D. Vlascici, G. Fagadar-Cosma, O. Bizerea and A. Chiriac, *Revista De Chimie*, 2004, **55**, 882-885.
49. K. H. Choi, J. Yoo, C. K. Lee and S. Y. Lee, *Energy & Environmental Science*, 2016, **9**, 2812-2821.
50. S. Aroua, T. K. Todorova, P. Hommes, L. M. Charnoreau, H. U. Reissig, V. Mougel and M. Fontecave, *Inorg. Chem.*, 2017, **56**, 5930-5940.

Figures

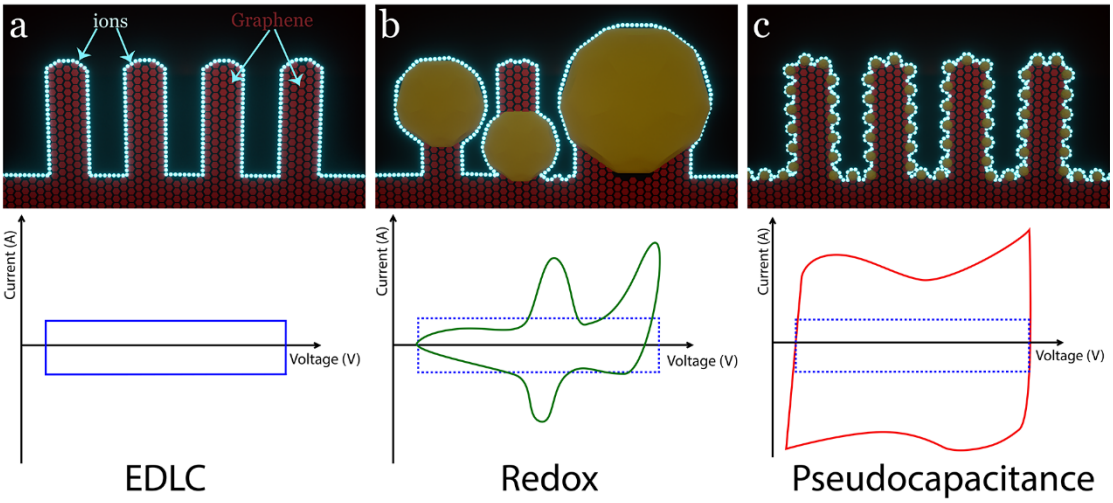

Schema 1 The illustration of cyclic voltammetry profiles according to different capacitive mechanism. (a) Pure graphene electrodes are dominated by electrical double layer capacitance. (b) Large additives on graphene electrodes result in battery-type redox peaks. (c) Nanosized additives on graphene electrodes contribute to pseudocapacitance.

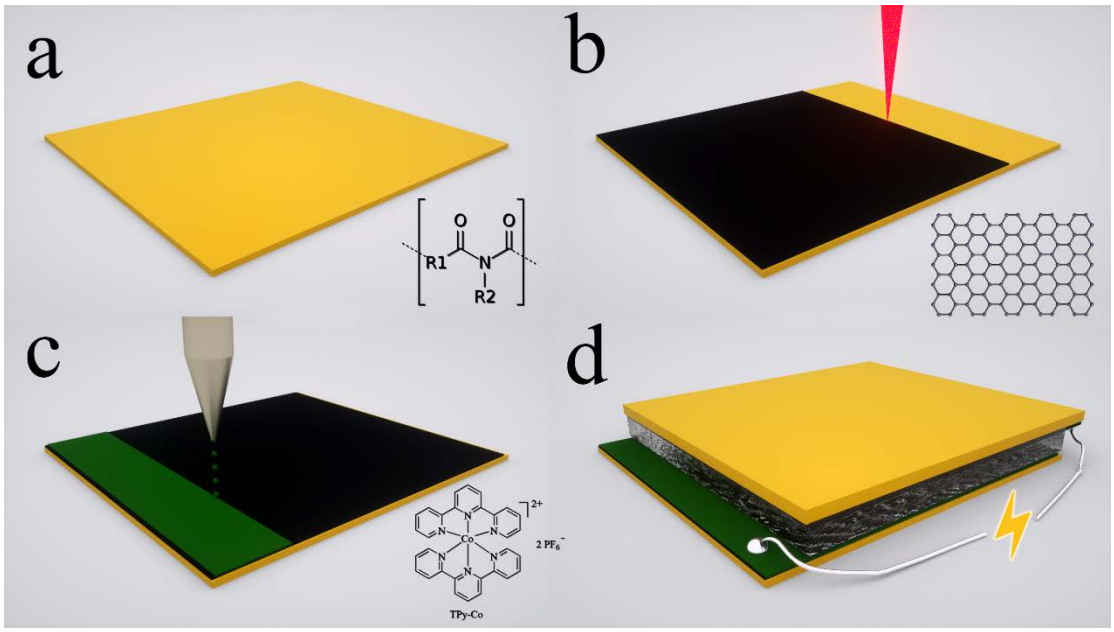

Figure 1 The overall process for fabricating the supercapacitor. (a) Pristine polyimide was used as the starting materials. (b) CO_2 laser scribing turned the polyimide into graphene. (c) Inkjet printing of TPy-Co inks on to the graphene as pseudocapacitive additives. (d) LiCl/PVA solid electrolyte was inserted between the two electrodes, as out-of-plane supercapacitor devices.

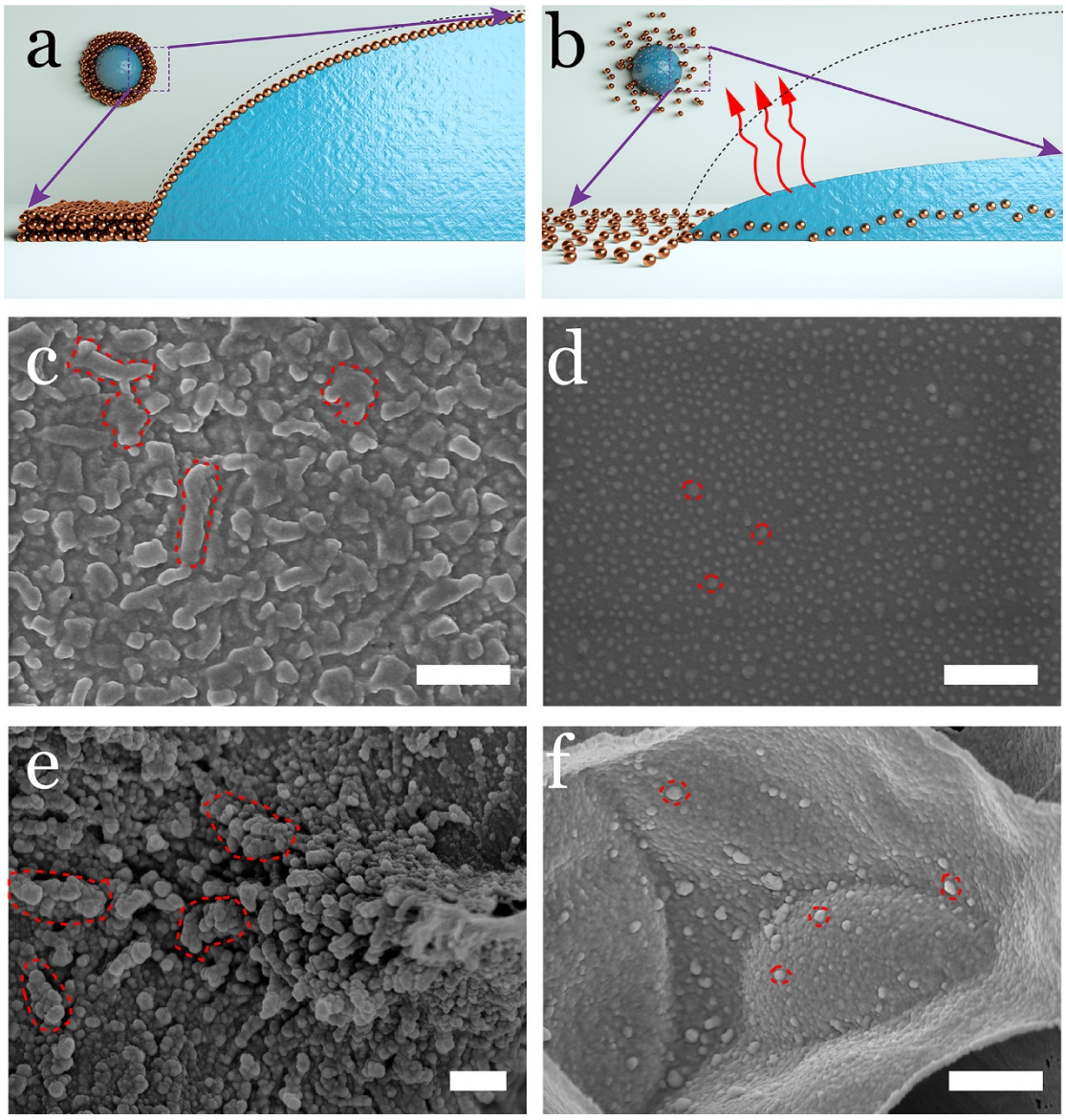

Figure 2. The influence of evaporating temperature on the distribution of solute in the droplet. (a) Coffee-ring distribution of solute in room temperature. (b) The eliminating of coffee ring effect when evaporating on high temperature. (c) The SEM image of the clogged TPy-Co solutes after inkjet printing on glass at room temperature. (d) The SEM image of the self-assembled TPy-Co solutes after inkjet printing on glass at solvent boiling temperature. (e) The SEM image of the clogged TPy-Co solutes after inkjet printing on laser-induced graphene at room temperature. (f) The SEM image of the separated TPy-Co solutes after inkjet printing on laser-induced graphene at high temperature. The scale bar is 500 nm in length.

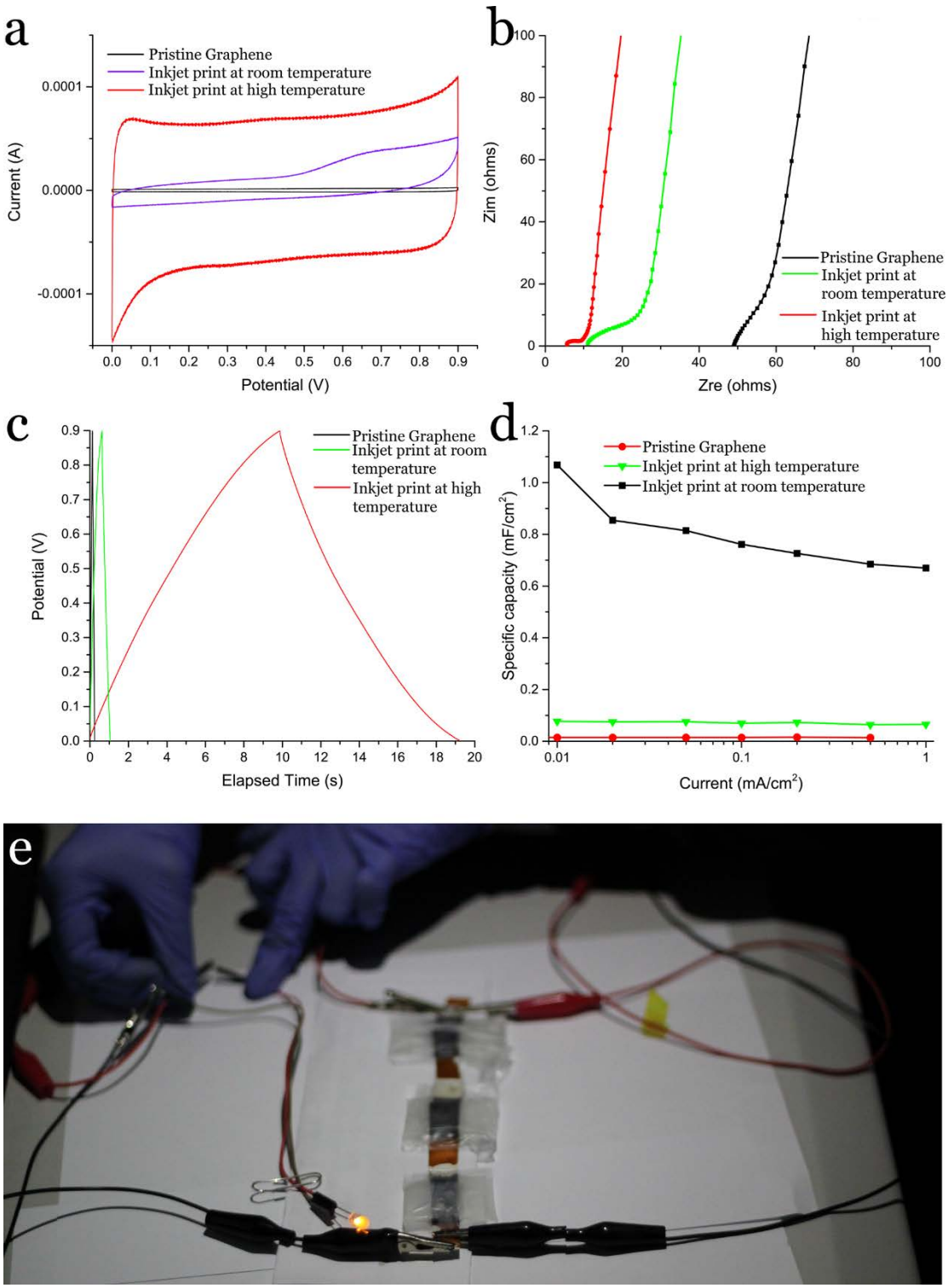

Figure 3. The electrochemical performance of the symmetry supercapacitor. (a) The measured cyclic voltammetry curves of the pristine graphene, with inkjet-printed TPy-Co at room temperature, and with inkjet-printed TPy-Co at high temperature with 100 mV/s scanning rates, respectively. (b) The EIS slop of the pristine graphene, with inkjet-

printed TPy-Co at room temperature, and with inkjet-printed TPy-Co at high temperature. (c) The galvanostatic charge/discharge curves of the pristine graphene, with inkjet-printed TPy-Co at room temperature, and with inkjet-printed TPy-Co at high temperature. (d) Comparison of specific capacitances with different inkjet printing conditions. (e) Three assembled inkjet-printed supercapacitors in series for powering up a LED.